ISSN 1674-1056
http://cpb.iphy.ac.cn
http://iopscience.iop.org/cpb
中国物理 B
Chinese Physics
中国物理
Chinese Physics B

Three-dimensional thermal illusion devices with arbitrary shape

Xingwei Zhang(张兴伟), Xiao He(何晓), Linzhi Wu(吴林志)

Citation: Chin. Phys. B . 2019, 28(6): 064403. **doi:** 10.1088/1674-1056/28/6/064403
Journal homepage: http://cpb.iphy.ac.cn; http://iopscience.iop.org/cpb

What follows is a list of articles you may be interested in

Contribution of terahertz waves to near-field radiative heat transfer between graphene-based hyperbolic metamaterials

Qi-Mei Zhao(赵启梅), Tong-Biao Wang(王同标), De-Jian Zhang(张德建), Wen-Xing Liu(刘文兴), Tian-Bao Yu(于天宝), Qing-Hua Liao(廖清华), Nian-Hua Liu(刘念华)

Chin. Phys. B . 2018, 27(9): 094401. **doi:** 10.1088/1674-1056/27/9/094401

Thermal properties of transition-metal dichalcogenide

Xiangjun Liu(刘向军), Yong-Wei Zhang(张永伟)

Chin. Phys. B . 2018, 27(3): 034402. **doi:** 10.1088/1674-1056/27/3/034402

General theories and features of interfacial thermal transport

Hangbo Zhou(周杭波), Gang Zhang(张刚)

Chin. Phys. B . 2018, 27(3): 034401. **doi:** 10.1088/1674-1056/27/3/034401

Two-dimensional thermal illusion device with arbitrary shape based on complementary media

Ge Xia(夏舸), Wei Kou(寇蔚), Li Yang(杨立), Yong-Cheng Du(杜永成)

Chin. Phys. B . 2017, 26(10): 104403. **doi:** 10.1088/1674-1056/26/10/104403

Thermal properties of two-dimensional materials

Gang Zhang(张刚), Yong-Wei Zhang(张永伟)

Chin. Phys. B . 2017, 26(3): 034401. **doi:** 10.1088/1674-1056/26/3/034401

Three-dimensional thermal illusion devices with arbitrary shape*

Xingwei Zhang(张兴伟)[1], Xiao He(何晓)[1,†], and Linzhi Wu(吴林志)[1,2,‡]

[1] *Key Laboratory of Advanced Ship Materials and Mechanics, College of Aerospace and Civil Engineering, Harbin Engineering University, Harbin* 150001, *China*

[2] *Center for Composite Materials, Harbin Institute of Technology, Harbin* 150001, *China*

(Received 14 January 2019; revised manuscript received 27 March 2019; published online 29 May 2019)

Since the concept of invisible cloak was proposed by Pendry and Leonhardt in 2006, many researchers have applied the theory of coordinate transformation to thermodynamics and overcome the complexity of inhomogeneous and anisotropic of material parameters. However, only two-dimensional (2D) thermal illusion devices are researched recently. According to this situation, our study focuses on three-dimensional (3D) thermal illusion devices including shrinker (or invisible cloak), concentrator, amplifier, reshaper, and rotator with arbitrary shape in a general way. In this paper, the corresponding material parameters of thermal illusion devices mentioned above are derived based on the theory of transformation thermodynamics and the simulated results agree well with the theoretical derivations. In addition, the conventional invisible cloak just controls the temperature gradient rather than the temperature value which is more concerned in physical applications. Here, we find that the temperature value of the cloaked object can be controlled by adjusting the location of the original point of the coordinate system.

Keywords: thermal illusion device, metamaterials, transformation thermaldynamics

PACS: 44.10.+I, 81.05.Xj, 07.05.Tp, 05.70.–a **DOI:** 10.1088/1674-1056/28/6/064403

1. Introduction

Heat energy which is full of mystery attracts researchers to explore the method of manipulating heat flux. According to the second law of thermodynamics, heat always flows from the hotter body to the colder one, which results in colossal difficulties for us to control heat flux. The hope is rooted in the concept of coordinate transformation that Pendry proposed in 2006 to design a device which makes object invisible towards electromagnetic waves.[1] The form-invariance of the corresponding physical equations[2,3] becomes the basic condition of coordinate transformation. Fortunately, many control equations have been proved to be form-invariant, which makes it possible to introduce coordinate transformation into other physical fields, such as microwave,[4] acoustics,[5,6] elastic waves,[7] mater waves,[8] and heat flux,[9] to design corresponding metastructures with fantastic functionalities. Based on the previous study, experts began to design thermal metastructures to control heat transfer in 2008. References [10] and [11] firstly proposed the idea of thermal invisible cloak and constructed the theory of transformation thermotics in steady state. With time passing by, Guenneau *et al.*[12] extended transformation thermotics from steady state to transient state in 2012 (named transformation thermodynamics), which made scientific community put more and more attention into the interesting issue. From then on, a series of novel thermal devices have been theoretically designed and experimentally realized,[13–31] such as thermal cloaks and thermal camouflages,[20,21] thermal concentrators,[9,18] thermal rotators,[9] and macroscopic thermal diodes,[15] *etc*., which open a fascinating door to control heat flux efficiently. In the process of fabricating metastructures, a sequence of approaches have been proposed to eliminate the inhomogeneity and singularities of the materials, including multilayered thermal devices based on effective medium theory[14,28] and a bilayer thermal cloak[13] based on scattering cancellation (or neutral inclusion theory.[20,22]) Meanwhile, a series of novel thermal illusion devices have been proposed in recent years. Reference [21] designed a thermal illusion device which could transform the thermal scattering signature of an arbitrary object to multiple isolated objects, and reference [32] realized a thermal illusion device which could transform a good thermal conductor to a poor one through the method of separation variables. References [33] and [34] designed thermal illusion devices based on the equation of heat conduction. At the process of designing thermal illusion devices, the method of coordinate transformation has played an important role. Based on coordinate transformation, references [35]–[38] reported a series of thermal illusion devices which could change the signature of heat source, including the position, the shape, or the quantity of heat source. Reference [27] designed a structure based on transformation thermotics which aimed at thermal radiation and was applicable to complex unknown environments.

However, the preceding studies mainly concentrate on the research of two-dimensional (2D) thermal illusion devices with arbitrary shape[30] and seldom discuss three-dimensional

*Project supported by the National Natural Science Foundation of China (Grant No. 11702069) and the Fundamental Research Funds for the Central Universities, China (Grant No. HEUCFM180203).

†Corresponding author. E-mail: hit_hx@163.com

‡Corresponding author. E-mail: wulinzhi@hrbeu.edu.cn

© 2019 Chinese Physical Society and IOP Publishing Ltd

(3D) cases except Ref. [29] (a spherical thermal cloak was proposed). It is necessary to extend thermal illusion devices from 2D to 3D random shape for the practical application of thermal metastructures. Therefore, this paper gives a general method to design 3D thermal illusion devices based on coordinate transformation, including thermal shrinker (or invisible cloak), concentrator, amplifier, reshaper and rotator theoretically and verifies the theoretical derivations through simulations.

2. Method

To construct the model of 3D thermal illusion devices with arbitrary shape in spherical coordinate, the inner and outer boundaries of the thermal illusion devices can be parameterized by varying radii[31]

$$r(\theta,\varphi) = A_{0,0} + \sum_{(m,n)\in N^2\setminus\{(0,0)\}} \Big\{A_{m,n}\cos(m\theta+n\varphi) + B_{m,n}\sin(m\theta+n\varphi)\Big\}, \quad (1)$$

where θ is the elevation angle and φ is the azimuth angle, m and n are the non-zero positive integer, $A_{0,0}$, $A_{m,n}$, and $B_{m,n}$ are arbitrary constants.

According to Fourier's law, the heat conduction equation without heat source is described by

$$\rho C\frac{\partial T}{\partial t} = \nabla\cdot(\kappa\nabla T), \quad (2)$$

where ρ is the density of medium, C is the specific heat capacity, and κ is the thermal conductivity of medium, and equation (2) keeps its form invariable under different coordinates. In this premise, multifarious thermal illusion devices can be designed by using different coordinate transformations to control heat flux.

A series of thermal devices can be designed through transforming (r,θ,φ) to (r',θ',φ'), where (r,θ,φ) and (r',θ',φ') represent virtual space and physical space, respectively, and different transformation equations correspond to different functional thermal devices. Then different thermal illusion devices can be proposed by deriving material parameters based on the theory of transformation thermodynamics. Figure 1 illustrates the general mode that constructs a series of illusion devices in a general way, and the functionalities of thermal illusion devices are different with each other when the surface c is located in different areas shown in Fig. 1.

In Fig. 1, a, b, and c denote the spatial surfaces, regions I ($c<r<b$ or $b<r<c$) and II ($0<r<c$) denote the virtual space, and regions III ($a<r<b$) and IV ($0<r<a$) denote the physical space Thermal illusion devices composed by "cloak" and "core" can be achieved by two steps: transforming c to a and keeping b unchanged (region I to region III); transforming c to a and keeping the origin point unchanged (region II to region IV). Region IV is the invisible object and region II is the corresponding illusion object. At the same time, it is the shrinker (or invisible cloak), the thermal concentrator, the thermal amplifier, and the thermal reshaper when surface c (or a point) is located in region IV, in region III, outside region III, and both in regions III and IV, respectively (the thermal reshaper can make the detected result changed from the real shape a to the shape c). One word to say, thermal illusion devices can make the thermal signal of region II alter to the one of region IV.

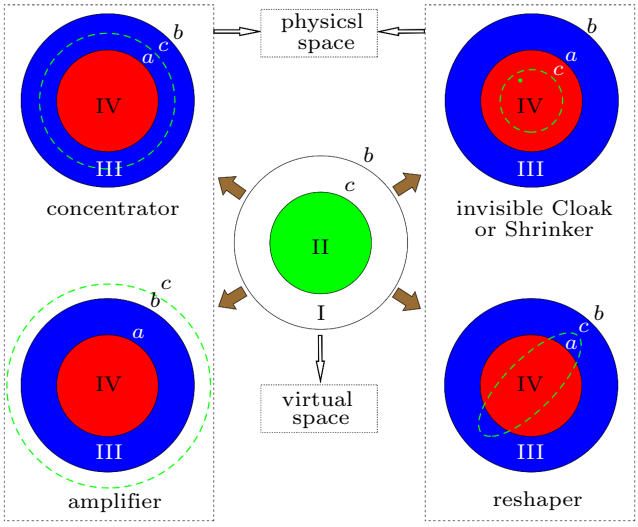


Fig. 1. Schematic illustration of transformations for thermal illusion devices. The virtual space and the physical space are constituted by regions I, II, and III, IV, respectively. a, b, and c denote the spatial curved surfaces.

Keeping θ and φ invariant and transforming r to r' (r and r' are dependent on θ, φ and θ', φ', respectively) in spherical coordinate system, the general expression of material parameters to fabricate thermal illusion devices including shrinker (or invisible cloak), concentrator, amplifier and reshaper can be derived through the transformation equations

$$r' = r\frac{b-a}{b-c} + b\frac{a-c}{b-c},\ \ \theta'=\theta,\varphi'=\varphi,\ \ (c<r<b), \quad (3)$$

$$r' = r\frac{a}{c},\theta'=\theta,\varphi'=\varphi,\ \ (r<c), \quad (4)$$

where a, b, and c are spatial curved surfaces described by Eq. (1). Equation (3) transforms region I into region III (that is to say, transforming c into a and holding b), and equation (4) transforms region II into region IV (transforming c into a and holding the original point). The transformation equations (3) and (4) can keep the material parameters continuous at boundaries and eliminate the interference on the gradient of the temperature field. It is noteworthy that for the invisible cloak, c is zero and only equation (3) is necessary.

According to Eqs. (3) and (4), the corresponding Jacobian matrixes are accurately derived as

$$\boldsymbol{J}_1 = \begin{bmatrix} A_{11} & A_{12} & A_{13} \\ 0 & A_{22} & 0 \\ 0 & 0 & A_{33} \end{bmatrix},\ \ \boldsymbol{J}_2 = \begin{bmatrix} B_{11} & B_{12} & B_{13} \\ 0 & B_{22} & 0 \\ 0 & 0 & B_{33} \end{bmatrix}, \quad (5)$$

where

$$\begin{cases} A_{11}=\dfrac{\partial r'}{\partial r}=\dfrac{b-a}{b-c},\ A_{12}=\dfrac{\partial r'}{r\partial\theta}=\dfrac{r'-b}{b-a}\cdot\dfrac{a'_\theta(c-b)+b'_\theta(a-c)+c'_\theta(b-a)}{r(b-c)}+\dfrac{b'_\theta(a-c)}{r(b-c)}, \\ A_{13}=\dfrac{\partial r'}{r\sin\theta\partial\varphi}=\dfrac{1}{\sin\theta}\left(\dfrac{r'-b}{b-a}\cdot\dfrac{a'_\varphi(c-b)+b'_\varphi(a-c)+c'_\varphi(b-a)}{r(b-c)}+\dfrac{b'_\varphi(a-c)}{r(b-c)}\right), \\ A_{22}=\dfrac{r'\partial\theta'}{r\partial\theta}=\dfrac{r'}{r},\ A_{33}=\dfrac{r'\sin\theta'\partial\varphi'}{r\sin\theta\partial\varphi}=\dfrac{r'}{r},\ r=r'\dfrac{b-c}{b-a}+b\dfrac{c-a}{b-a},\ \theta=\theta', \end{cases}$$

$$\begin{cases} B_{11}=\dfrac{\partial r'}{\partial r}=\dfrac{a}{c},\ B_{12}=\dfrac{\partial r'}{r\partial\theta}=\dfrac{a'_\theta c-c'_\theta a}{c^2},\ B_{13}=\dfrac{\partial r'}{r\sin\theta\partial\varphi}=\dfrac{a'_\varphi c-c'_\varphi a}{c^2\sin\theta}, \\ B_{22}=\dfrac{r'\partial\theta'}{r\partial\theta}=\dfrac{r'}{r},\ B_{33}=\dfrac{r'\sin\theta'\partial\varphi'}{r\sin\theta\partial\varphi}=\dfrac{r'}{r},\ r=r'\dfrac{c}{a},\ \theta=\theta', \end{cases}$$

and $f'_\theta=\dfrac{\partial f}{\partial\theta}$, $f'_\varphi=\dfrac{\partial f}{\partial\varphi}$, $f=a,b,c$.

According to Ref. [31] and Eq. (5), the material parameters of regions III and IV can be derived as

$$\boldsymbol{\kappa}^{\mathrm{III}}=\frac{\boldsymbol{J}_1\boldsymbol{\kappa}^{\mathrm{I}}\boldsymbol{J}_1^{\mathrm{T}}}{\det\boldsymbol{J}_1},\ (\rho C)^{\mathrm{III}}=\frac{(\rho C)^{\mathrm{I}}}{\det\boldsymbol{J}_1}, \tag{6}$$

$$\boldsymbol{\kappa}^{\mathrm{IV}}=\frac{\boldsymbol{J}_2\boldsymbol{\kappa}^{\mathrm{II}}\boldsymbol{J}_2^{\mathrm{T}}}{\det\boldsymbol{J}_2},\ (\rho C)^{\mathrm{IV}}=\frac{(\rho C)^{\mathrm{IV}}}{\det\boldsymbol{J}_2}, \tag{7}$$

where $\boldsymbol{\kappa}^i$, ρ^i, C^i, and $(\rho C)^i$ ($i=$ I, II, III, and IV) are the thermal conductivity, the density, the specific heat capacity, and the product of ρ^i and C^i in the region i, respectively, and the superscript "T" denotes transposed matrix. In view of the real situation that usually the parameters of the cloaked object (region IV) are known rather than the one of the illusion object (region II), equation (7) can be converted into

$$\boldsymbol{\kappa}^{\mathrm{II}}=\boldsymbol{J}_2^{-1}\boldsymbol{\kappa}^{\mathrm{IV}}\boldsymbol{J}_2^{-\mathrm{T}}\det\boldsymbol{J}_2,\ (\rho C)^{\mathrm{II}}=(\rho C)^{\mathrm{IV}}\det\boldsymbol{J}_2. \tag{8}$$

Equations (6) and (8) are the general expressions of material parameters for arbitrary 3D thermal illusion devices mentioned above. After that, we also proposed an arbitrary 3D rotator (Fig. 1) by transforming φ to φ' and keeping r and θ invariant, and the transformation equations can be chosen as

$$r'=r,\ \theta'=\theta,\ \varphi'=\varphi+\varphi_0\frac{b-r}{b-a},\ (a<r<b), \tag{9}$$

$$r'=r,\ \theta'=\theta,\ \varphi'=\varphi+\varphi_0,\ (r<b), \tag{10}$$

where φ_0 is the degree of rotation of heat flux. The corresponding material parameters of the core and cloak can be derived by Eq. (6) where the Jacobian matrixes should be changed.

For facility of simulations based on the finite element method, the material parameters in the Cartesian coordinate system are derived by the following Jacobian matrix:

$$\boldsymbol{J}=\begin{bmatrix}\cos\varphi\sin\theta & \cos\varphi\cos\theta & -\sin\varphi\\ \sin\varphi\sin\theta & \cos\theta\sin\varphi & \cos\varphi\\ \cos\theta & -\sin\theta & 0\end{bmatrix}, \tag{11}$$

where θ and φ are the elevation angle and azimuth angle, and the corresponding thermal conductivity can be expressed as

$$\boldsymbol{\kappa}_{\mathrm{r}}^i=\boldsymbol{J}\boldsymbol{\kappa}^i\boldsymbol{J}^{\mathrm{T}}=\begin{bmatrix}\kappa_{xx}^i & \kappa_{xy}^i & \kappa_{xz}^i\\ & \kappa_{yy}^i & \kappa_{yz}^i\\ \mathrm{sym} & & \kappa_{zz}^i\end{bmatrix},\ i=\mathrm{II},\ \mathrm{III}, \tag{12}$$

where

$$\begin{aligned}
\kappa_{xx}^i&=\left(\kappa_{11}^i\sin^2\theta+\kappa_{12}^i\sin2\theta+\kappa_{22}^i\cos^2\theta\right)\cos^2\varphi\\
&\quad-\kappa_{13}^i\sin2\varphi\sin\theta+\kappa_{33}^i\sin^2\varphi,\\
\kappa_{xy}^i&=\left(\kappa_{11}^i\sin^2\theta+\kappa_{12}^i\sin2\theta+\kappa_{22}^i\cos^2\theta-\kappa_{33}^i\right)\sin\varphi\cos\varphi\\
&\quad+\kappa_{13}^i\cos2\varphi\sin\theta,\\
\kappa_{xz}^i&=\left(\left(\kappa_{11}^i-\kappa_{22}^i\right)\sin\theta\cos\theta+\kappa_{12}^i\cos2\theta\right)\cos\varphi\\
&\quad-\kappa_{13}^i\cos\theta\sin\varphi,\\
\kappa_{yy}^i&=\left(\kappa_{11}^i\sin^2\theta+\kappa_{12}^i\sin2\theta+\kappa_{22}^i\cos^2\theta\right)\sin^2\varphi\\
&\quad+\kappa_{13}^i\sin2\varphi\sin\theta+\kappa_{33}^i\cos^2\varphi,\\
\kappa_{yz}^i&=\left(\left(\kappa_{11}^i-\kappa_{22}^i\right)\sin\theta\cos\theta+\kappa_{12}^i\cos2\theta\right)\sin\varphi\\
&\quad+\kappa_{13}^i\cos\theta\cos\varphi,\\
\kappa_{zz}^i&=\kappa_{11}^i\cos^2\theta-\kappa_{12}^i\sin2\theta+\kappa_{22}^i\sin^2\theta,
\end{aligned}$$

and the subscript "r" means Cartesian coordinate system

3. Simulation

Since the necessary material parameters for designing the thermal illusion devices have been given above, the simulations conducted in the finite element software COMSOL Multiphysics will be introduced hereafter to display and verify the theoretical results mentioned above. To decrease the load of calculation and without loss of generality, it is enough to analyze arbitrary thermal illusion devices built with surfaces of revolution, *i.e.*, generated by rotating a curve about the z-axis. In this paper, we discuss the design of axially invariant 3D devices with an arbitrary cross-section described by variable radii $r(\theta)$ that gives an angle dependent distance from the origin. According to Eq. (1), the radii can be simplified as

$$r(\theta)=A_0+\sum_{m=1}^{M}\{A_m\cos m\theta+B_m\sin m\theta\}, \tag{13}$$

where M can be a small integer. For the generalization, the boundaries of the shrinker (or invisible cloak), concentrator, amplifier, reshaper, and rotator have been designed by different equations described by Eq. (13), that is to say, the derivation is effective for arbitrary shapes.

In the process of simulation, the background region is a cuboid, the left and right boundary conditions of the cuboid are 600 K and 300 K, respectively, the other boundary conditions are insulation, and the isothermal lines are denoted by the

white lines in the simulation results. For the cases of thermal invisible cloak, concentrator, and rotator, the parameters have been set as $\kappa^{\mathrm{I}} = 0.025\ \mathrm{W}\cdot(\mathrm{mK})^{-1}$, $\rho^{\mathrm{I}} = 1.293\ \mathrm{kg}\cdot\mathrm{m}^{-3}$ and $C^{\mathrm{I}} = 1.4\ \mathrm{kJ}\cdot(\mathrm{kg}\cdot\mathrm{K})^{-1}$ in Eq. (6), and given $\kappa^{\mathrm{IV}} = 0.025\ \mathrm{W}\cdot(\mathrm{mK})^{-1}$, $\rho^{\mathrm{IV}} = 1.293\ \mathrm{kg}\cdot\mathrm{m}^{-3}$, and $C^{\mathrm{IV}} = 1.4\ \mathrm{kJ}\cdot(\mathrm{kg}\cdot\mathrm{K})^{-1}$ in Eq. (8). And for the thermal amplifier and reshaper, the parameters have been set as $\kappa^{\mathrm{I}} = 400\ \mathrm{W}\cdot(\mathrm{mK})^{-1}$, $\rho^{\mathrm{I}} = 8960\ \mathrm{kg}\cdot\mathrm{m}^{-3}$ and $C^{\mathrm{I}} = 385\ \mathrm{kJ}\cdot(\mathrm{kg}\cdot\mathrm{K})^{-1}$ (copper) in Eq. (6), where the superscripts I and IV denote the material parameters of the background and the cloaked object, respectively.

The shape of the simulated thermal invisible cloak is displayed in Fig. 2, where figure 2(a) is the basic profile of the cross-section in xz plane and figure 2(b) is the schematic illustration of the simulated sample. To keep the geometrical continuity at the joint of the slant line and the arc, the slant line is tangent to the arc, and the invisible cloak is divided into three sections (1, 2, and 3) by two lines through the original point (the dotted line in Fig. 2(a)). The corresponding material parameters of each section can be derived based on Eqs. (6) and (12), where $c = 0$.

Without loss of generality, a rotational solid similar to the top of a missile has been embedded into an isotropic homogeneous cuboid background material. Parameters of the cloak ($a < r < b$ in Fig. 2) are derived by Eqs. (6) and (12), and the interior material (cloaked object) of the cloak is the same as the background one. The simulation results at the time $t = 4000$ s, $t = 10000$ s and steady state are shown in Fig. 3 and for comparison the corresponding results of a reference sample without a cloak are shown in Figs. 3(a1)–3(a3) and 3(b1)–3(b3). Comparing these results in Fig. 3, it is easy to find that the heat gradient is zero in the cloaked region when the contours of the temperature field detour around the cloaked object perfectly without disturbing the temperature field in the background, which looks like that nothing is there, just as same as the reference sample. Benefiting from the invisible cloak, not only a uniform temperature value can be achieved in the cloaked region, but also no disturbance is introduced into the background material.

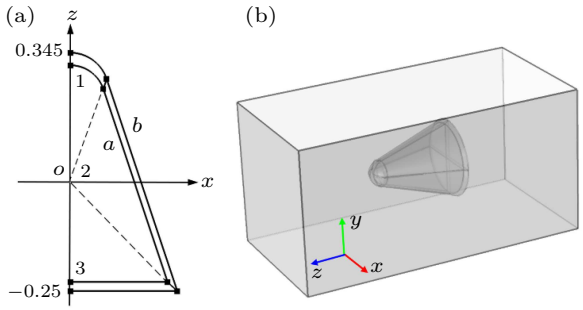


Fig. 2. The geometry model of a 3D arbitrary invisible cloak. Panel (a) is the basic profile of the invisible cloak with boundaries a and b. Panel (b) is the schematic illustration of the simulated sample.

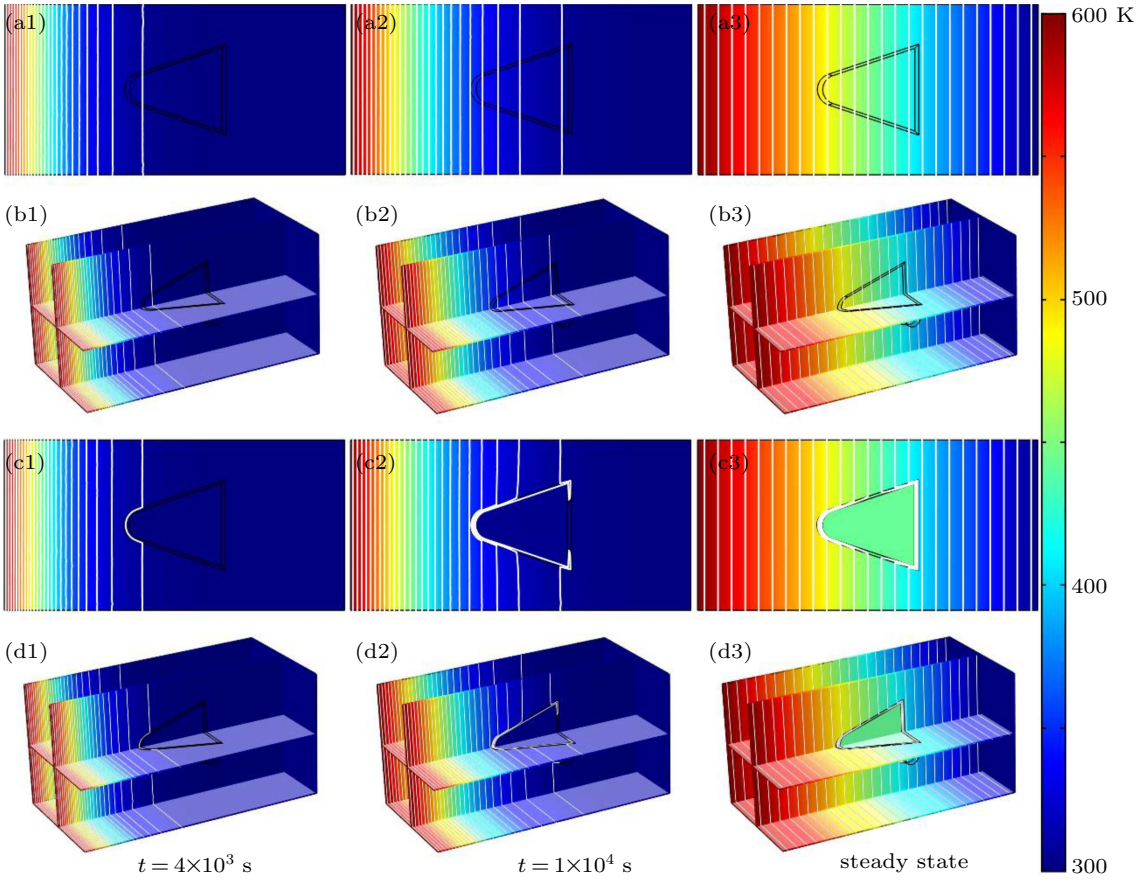


Fig. 3. The simulation results of a thermal invisible cloak. Panels (a1)–(a3) and (b1)–(b3) are the 2D and 3D simulation results of the reference sample without a cloak, respectively. Panels (c1)–(c3) and (d1)–(d3) are the corresponding 2D and 3D simulated results of the situation with an invisible cloak, respectively.

In addition, another interesting phenomenon shows that the temperature of the cloaked object will vary with the location of the original point of the coordinate system and the temperature value in the core is equal to the temperature value in the $z = 0$ plane. In order to explore the problem of controlling the temperature value rather than the thermal gradient, the location of the original point in Fig. 2 has been set at the top, the middle, and the bottom of the cloaked object and the corresponding steady-state simulated results are displayed in Fig. 4. Figures 4(b1)–4(b3) and 4(c1)–4(c3) are the 2D and 3D steady-state temperature distributions of the simulated results with different original points, respectively, the same colors denote the same temperature values, and the black lines in Figs. 4(b1)–4(b3) denote the $z = 0$ planes. As illustrated in Fig. 4, the corresponding temperature values of the cloaked object are 478.7 K, 443.2 K, and 420.8 K when the origin point is located in the top, the middle, and the bottom of the cloaked object, and equal the temperature values of the $z = 0$ plane. In other words, the local temperature value can be expanded to a space through coordinate transformation in the process of heat conduction. This phenomenon is attributed to the process of coordinate transformation. To design the invisible cloak, one point (the green point in Fig. 1) should be extended to a space, such that the heat flow passes through this space just like going through the green point (that is to say, without any disturbances introduced in). Therefore, the temperature value of the whole core is the same as the one of the isothermal surface which the green point (Fig. 1) was located in. Consequently, the temperature of the core will change with the location of the green point (the original point here).

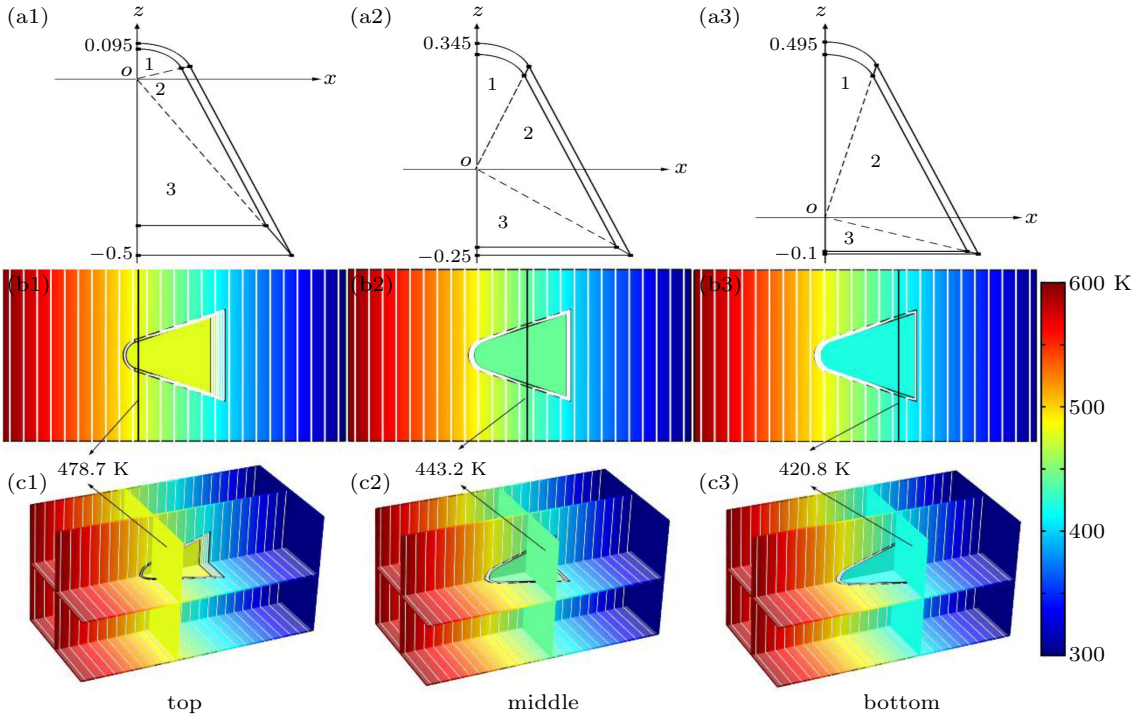


Fig. 4. Controlling of the temperature of the cloaked object by adjusting the location of the original point. Panels (a1)–(a3) are different locations of the original points. Panels (b1)–(b3) and (c1)–(c3) are the 2D and 3D steady state temperature distributions of the simulated results with different original points, respectively.

To further demonstrate the validity and generality of the derivations in this paper, the simulation of a thermal concentrator (with boundaries a, b, and c) has been carried out as well. The simulated configuration and results of the thermal concentrator are illustrated in Figs. 5 and 6 respectively. For comparison, both the concentrator and a reference sample have been studied. Then, the parameters of the core ($r < a$) and the cloak ($a < r < b$) can be derived by Eqs. (6) and (8), respectively. Figure 6 shows the simulation results (in the yz plane) both in transient (the first two columns) and steady state (the last column). Comparing the simulation results of the concentrator (Figs. 6(c1)–6(c3) and 6(d1)–6(d3)) and the one of reference sample (Figs. 6(a1)–6(a3) and 6(b1)–6(b3)), it is clear that the concentrator can absorb heat flux without disturbing the heat flux in the background material both in transient and steady state, which may be used to harvest energy in the future.

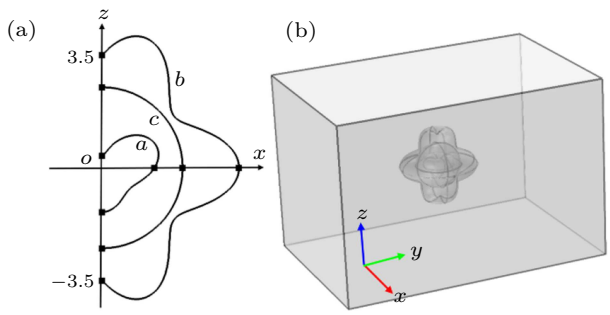


Fig. 5. The simulated configuration of a concentrator. Panel (a) is the basic profile of the concentrator. Panel (b) is the schematic illustration of the simulated sample.

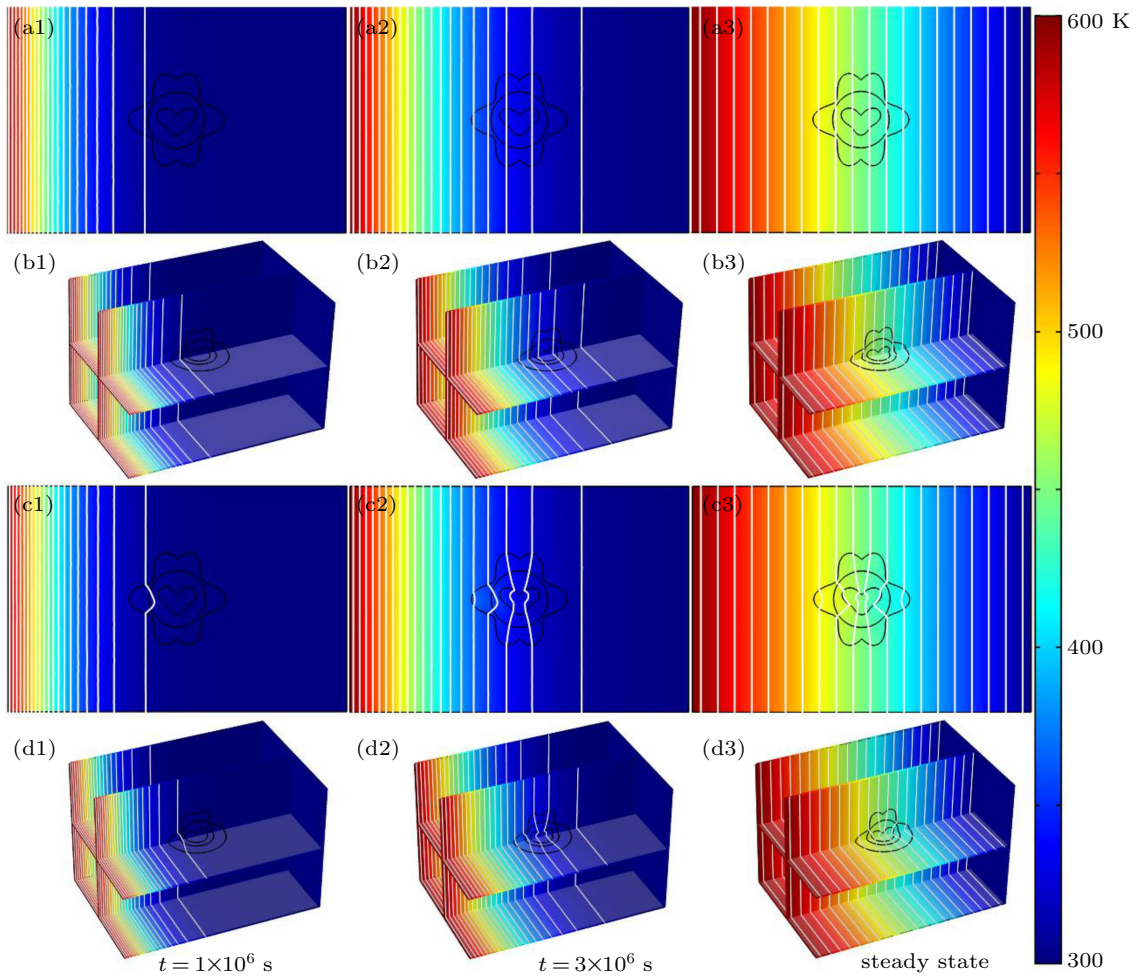


Fig. 6. The simulation results of a thermal concentrator. Panels (a1)–(a3) and (b1)–(b3) are the 2D and 3D simulation results of the reference sample without a concentrator, respectively. Panels (c1)–(c3) and (d1)–(d3) are the 2D and 3D simulation results of the concentrator worked sample, respectively.

Meanwhile, a thermal amplifier has been constructed by the same method. The basic simulation model and results are illustrated in Figs. 7 and 8. In Fig. 7, the region $r < a$ denotes the actual object, and the region $a < r < b$ denotes the amplifier. It should be noted that the region $b < r < c$ is virtual, and the $r = c$ boundary only denotes the shape of the illusion object. To design the thermal amplifier, the parameters of cloak can be derived by Eqs. (3), (6), and (12). Figures 8(a1), 8(b1) and 8(a2), 8(b2) are the simulation results of actual object and amplifier, respectively, figures 8(a3) and 8(b3) are the simulation results of illusion object, and figures 8(a1)–8(a3) are the distributions of temperature field in yz plane. It is clear that the thermal signature of the amplified object is the same as the one of illusion object, and bigger than the one of actual object. That is to say, the thermal amplifier amplifies the thermal signature of actual object. This can make the detectors get the inaccurate thermal signature.

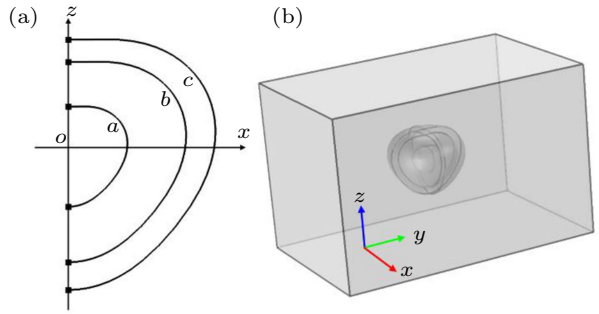


Fig. 7. The geometry model of a 3D arbitrary thermal amplifier. Panel (a) is the basic profile of the cross-section in xz plane of the amplifier. Panel (b) is the schematic illustration of the simulated sample, and the cuboid denotes the background material (copper).

Furthermore, a thermal reshaper constructed by Eqs. (3), (6), and (12) is illustrated in Fig. 9, and the region $r < a$ denotes the actual object, the region $a < r < b$ denotes the reshaper, and the boundary $r = c$ denotes the shape of the illusion object. The materials of actual object and background are the same as the case of thermal amplifier. The 2D and 3D simulation results are displayed in Fig. 10. As illustrated in Fig. 10, figures 10(a1), 10(b1) and 10(a2), 10(b2) are the simulation results of actual object and reshaper, respectively, figures 10(a3) and 10(b3) are the simulation results of illusion object, and fig-

ures 10(a1)–10(a3) are the distributions of temperature field in xz plane . Under the action of thermal reshaper, the thermal distribution of actual object is the same as the one of illusion object. In other words, the thermal signature of actual object in Figs. 10(a1) and 10(b1) has been changed to the one of illusion object in Figs. 10(a3) and 10(b3). The detectors will observe the inaccurate shape when the thermal reshaper works on.

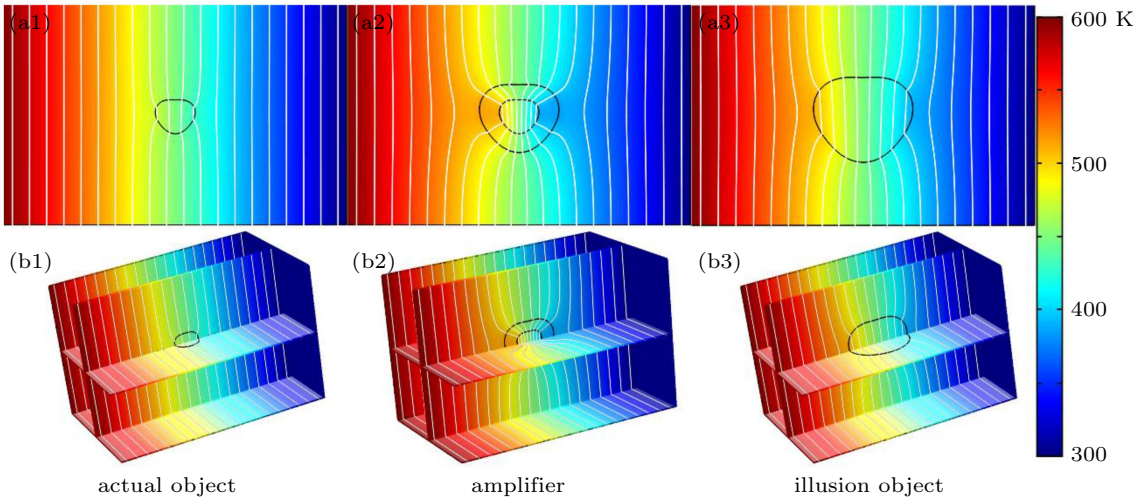


Fig. 8. The simulation results of a thermal amplifier. Panels (a1)–(a3) are the 2D simulation results in the yz plane ($x = 0$), and panels (b1)–(b3) are the 3D simulation results.

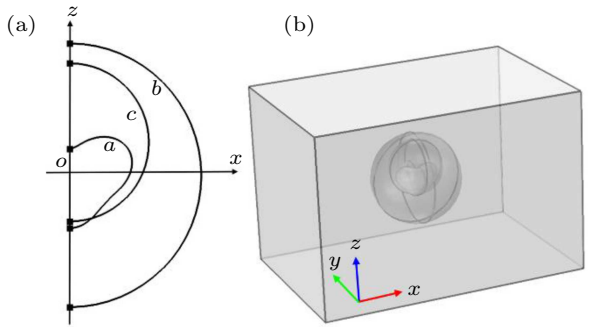


Fig. 9. The simulated configuration of a reshaper. Panel (a) is the basic profile of the cross section of the reshaper. Panel (b) is the reshaper that has been placed into a cuboid.

At last, a thermal rotator (with boundaries a and b) can be designed by the general method mentioned above through the transformation Eqs. (9) and (10), and the corresponding material parameters of the cloak ($a < r < b$) and core ($r < a$) are derived by Eqs. (6) and (8), respectively. The schematic diagram and the simulation results of the rotator are illustrated in Figs. 11 and 12. Comparing the distributions of the temperature of the rotator and the reference sample in the xy plane at $z = 2.5$ and $z = 0$ (Fig. 12), it is obvious that the thermal rotator rotates the parallel isothermal lines into $\pi/3$ degree and without disturbing the distribution of the thermal field in the background material. It should be noted that the degree of rotation can be changed discretionarily, and in this case, the degree is set as $\pi/3$.

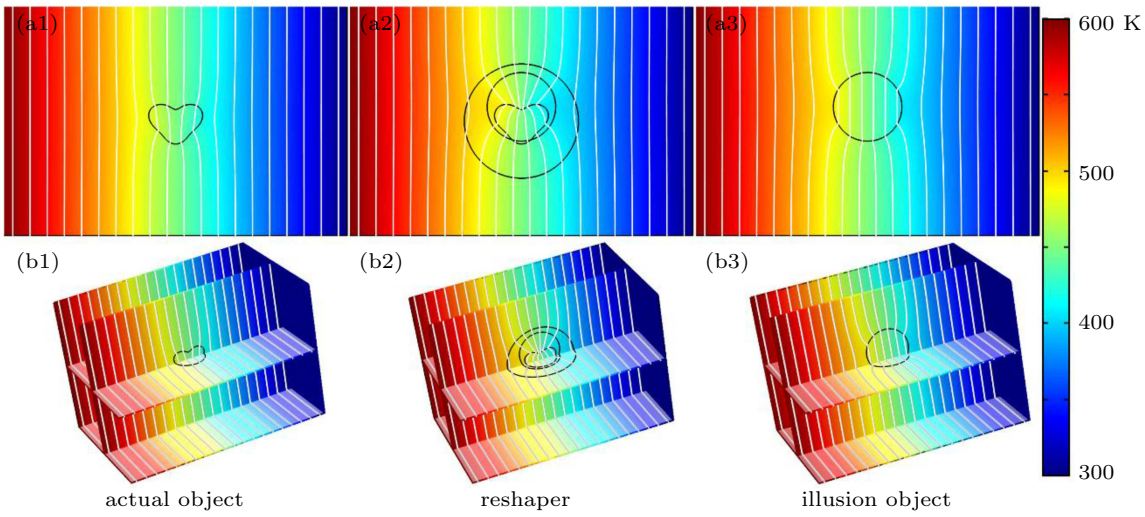


Fig. 10. The simulation results of thermal reshaper. Panels (a1)–(a3) and (b1)–(b3) are the 2D and 3D simulation results in the xz plane ($y = 0$), respectively.

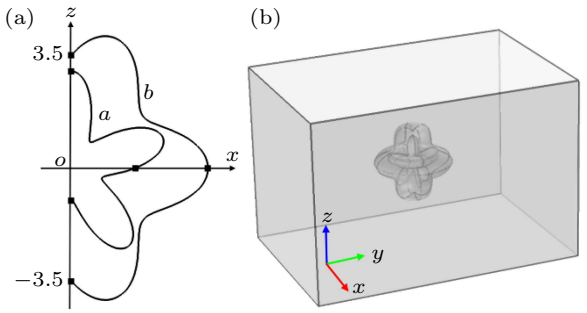


Fig. 11. The simulated configuration of a rotator. Panel (a) is the basic profile of the cross section of the rotator. Panel (b) is the schematic illustration of the simulated sample.

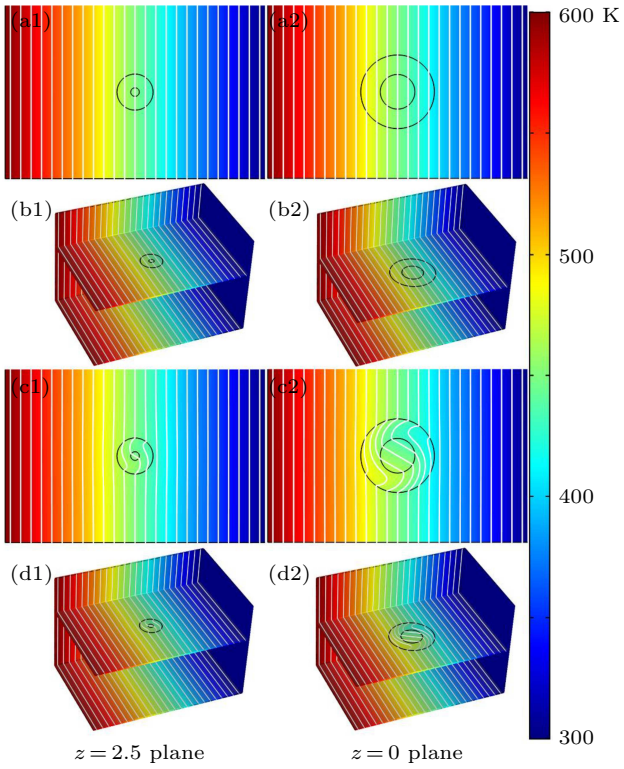


Fig. 12. The distribution of temperature in different cut planes (rotator). The two columns represent the temperature contours at $z = 2.5$ and $z = 0$, respectively. Panels (a1), (a2), (b1), and (b2) are the simulation results of the reference sample without a rotator. Panels (c1), (c2), (d1), and (d2) are the simulation results of the rotator worked sample.

4. Conclusion

This paper proposes a general way to fabricate 3D thermal illusion devices with arbitrary cross section including thermal shrinker (or invisible cloak), concentrator, amplifier, reshaper, and rotator based on the theory of transformation thermodynamics. All the thermal illusion devices motioned above have been successfully simulated to verify the validity and efficiency of the theoretical derivations by finite element method. Simultaneously, the influence of the location of the coordinate origin on the temperature value of the cloaked object has been discussed. It is found that the temperature value of the cloaked object can be manipulated by adjusting the location of the origin point, and this phenomenon should be used to design the metamaterials with the function of guiding heat flux from higher temperature (or lower temperature) to lower temperature (or higher temperature) autonomously without forcing energy source on the cloak. This phenomenon is not only limited to the thermodynamics, but also it can be generalized into other physical fields, which can be used to control the internal signal rather than eliminating the external disturbance only.

References

[1] Pendry J B, Schurig D and Smith D R 2006 *Science* **312** 1780
[2] Lax M and Nelson D F 1976 *Phys. Rev. B* **13** 1777
[3] Shalaev V M 2008 *Science* **322** 384
[4] Schurig D, Mock J J, Justice B J, Cummer S A, Pendry J B, Starr A F and Smith D R 2006 *Science* **314** 977
[5] Zhang S, Xia C G and Fang N 2011 *Phys. Rev. Lett.* **106** 024301
[6] Popa B I, Zigoneanu L and Cummer S A 2011 *Phys. Rev. Lett.* **106** 253901
[7] Brun M, Guenneau S and Movchan A B 2009 *Appl. Phys. Lett.* **94** 061903
[8] Zhang S, Genov D A, Sun C and Zhang X 2008 *Phys. Rev. Lett.* **100** 123002
[9] Narayana S and Sato Y 2012 *Phys. Rev. Lett.* **108** 214303
[10] Fan C Z, Gao Y and Huang J P 2008 *Appl. Phys. Lett.* **92** 251907
[11] Chen T Y, Weng C N and Chen J S 2008 *Appl. Phys. Lett.* **93** 114103
[12] Guenneau S, Amra C and Veynante D 2012 *Opt. Express* **20** 8207
[13] Han T C, Bai X, Gao D L, Thong J T L, Li B W and Qiu C W 2014 *Phys. Rev. Lett.* **112** 054302
[14] Schittny R, Kadic M, Guenneau S and Wegener M 2013 *Phys. Rev. Lett.* **110** 195901
[15] Li Y, Shen X Y, Wu Z H, Huang J Y, Chen Y X, Ni Y S and Huang J P 2015 *Phys. Rev. Lett.* **115** 195503
[16] Shen X Y, Li Y, Jiang C R and Huang J P 2016 *Phys. Rev. Lett.* **117** 055501
[17] Yang T Z, Su Y S, Xu W K and Yang X D 2016 *Appl. Phys. Lett.* **109** 120905-1
[18] Shen X Y, Y Li, Jiang C R, Ni Y S and Huang J P 2016 *Appl. Phys. Lett.* **109** 031907
[19] Shen X Y, Jiang C R, Li Y and Huang J P 2016 *Appl. Phys. Lett.* **109** 201906
[20] He X, Yang T Z, Zhang X W, Wu L Z and He X Q 2017 *Sci. Rep.* **7** 16671
[21] Han T C, Bai X, Thong J T L, Li B W and Qiu C W 2014 *Adv. Mater.* **26** 1731
[22] He X and Wu L Z 2013 *Phys. Rev. E* **88** 033201
[23] Maire J, Anufriev R, Yanagisawa R, Ramiere A, Volz S and Nomura M 2017 *Sci. Adv.* **3** E1700027
[24] Hamed A and Ndao S 2018 *Int. J. Heat Mass Transfer* **121** 10
[25] Shang J, Wang R Z, Xin C, Dai G L and Huang J P 2018 *Int. J. Heat Mass Transfer* **121** 321
[26] Wang R Z, Xu L J, Ji Q and Huang J P 2018 *J. Appl. Phys.* **123** 115117
[27] Li Y, Bai X, Yang T Z, Luo H L and Qiu C W 2018 *Nat. Commun.* **9** 273
[28] He X, Yang T Z and Wu L Z 2018 *J. Heat Transfer* **140** 102001
[29] Xu H Y, Shi X H, Gao F, Sun H D and Zhang B L 2014 *Phys. Rev. Lett.* **112** 054301
[30] He X and Wu L Z 2014 *Appl. Phys. Lett.* **105** 221904
[31] Dupont G, Guenneau S, Enoch S, Demesy G, Nicolet A, Zolla F and Diatta A 2009 *Opt. Express* **17** 22603
[32] Chen T H, Yang F and Mei Z L 2015 *Physica Status Solidi A* **212** 1746
[33] Wang R, Xu L J and Huang J P 2017 *J. Appl. Phys.* **122** 215107
[34] Yang S, Xu L J, Wang R Z and Huang J P 2017 *Appl. Phys. Lett.* **111** 121908
[35] Hou Q W, Zhao X P, Meng T and Liu C L 2016 *Appl. Phys. Lett.* **109** 103506
[36] Zhou S L, Hu R and Luo X B 2018 *Int. J. Heat Mass Transfer* **127** 607
[37] Hu R, Zhou S L, Li Y, Lei D Y, Luo X B and Qiu C W 2018 *Adv. Mater.* **30** 1707237
[38] Xu L J and Huang J P 2018 *Phys. Lett. A* **382** 3313